LOCATING SPECTRA ON THE FOS DIGICONS AND THE PHOTOMETRIC CONSEQUENCES OF ERRORS IN POSITION*

J. WHEATLEY and R. BOHLIN

SPACE TELESCOPE SCIENCE INSTITUTE

Instrument Science Report CAL/FOS-022

October, 1985

Prelim Draft

I. Inroduction

The optimum method of determining the locations and orientations of FOS spectra on the two-dimensional Digicon photocathodes is investigated. The Y-center of a spectrum as a function of diode number deviates from linearity by up to 15 microns because of small distortions in the magnetic focusing fields in the Digicons. In addition, the spectra are rotated by small angles (typically $0.^{\circ}05$ for the high resolution gratings) with respect to the diode array. This report presents all spectral position and orientation measurements since the replacement of the Digicons in the second quarter of 1984. Average shifts in spectral position are computed between calibrations at different temperatures and at different Digicon voltages.

The photometric effect of errors in Y-position could not be determined directly to better than 5 percent from the observed Pt-Cr-Ne emission line spectra. However, the light loss caused by an incorrect Y-center can be modeled using the mean point source cross-sections and the mean loci of Y-centers. Examples of *observed* light loss curves derived from high signal-to-noise external Tungsten lamp *continuum* spectra are presented. These results will provide a useful check on the subsequent modeling.

* *The red Digicon used for this study developed a large internal gas pressure and was removed from the FOS in September, 1985. The results discussed here should be considered as only illustrative of what the red replacement tube might be.*

II. Location of Spectra

A. Definition of Y-base and Theta-Z

In order to determine the center of a spectrum on the photocathode, the diode array is stepped perpendicular to the dispersion to make a Y-map. The standard procedure in ground calibrations was to use 24 Y-steps covering a range of 384 microns, resulting in an image with a step size of 16 microns in Y, and 512 pixels on 50 micron centers in X. The Y-map is centered on the expected position of the spectrum. We are interested in computing two parameters from the Y-map: 1) the optimum Y-deflection for acquiring the spectrum, referred to as the Y-base, and 2) the angle that the spectrum makes relative to the diode array, designated theta-Z.

The optimum Y-deflection is determined in the following manner. Once the Y-center of the spectrum is known as a function of diode number, a linear curve is fit to the points. The data points that define the Y-center can deviate from a straight line because of small distortions in the magnetic focusing fields. The linear fit is then used to define the Y-base. When the entire diode array is covered by a spectrum, the Y-base is evaluated at diode 256, the X-center of the array. For other dispersers, where only part of the diode array is used, the Y-base is evaluated at the center of the spectrum. These central X-positions are tabulated for all disperser/tube combinations in Table 1. Examples of Y-center curves and best fit lines are shown in Figures 1-4. Y-bases are measured in "Y-base units", which correspond to microns to within 10%. The angle theta-Z is defined as the arctangent of the slope of the best fit line.

B. Algorithms for Determining the Y-center of Spectra

Considerable thought was given to the problem of devising a general algorithm to determine the Y-center as a function of X. Since the prime method of determining Y-bases uses the on-board Pt-Cr-Ne lamps and since many regions of interest contain few bright emission lines, the algorithm must work well on low signal-to-noise data. Furthermore, many spectra are not well centered in the Y-map, so that the algorithm should be insensitive to truncation of a Y cross-section. The shapes of the cross-sections in Y vary with aperture size from the square shape shown in Figure 5 to the triangular form shown in Figure 6. Three methods for determining the center of such curves were considered: 1) cross-correlation, 2) centroiding, and 3) contour averaging. The cross-correlation method was selected, because it produced the best results for low signal levels. The merits of each method are briefly discussed in the following sections.

i. Cross-correlation

A square template is cross-correlated with the Y cross-section to determine the point of best correlation which defines the center of the spectrum. In order to improve the counting statistics, the spectra are summed in 51 diode bins, resulting in 10 data points per spectrum in X. The bin size is a compromise between the need to produce smooth cross-sections in regions of the spectrum with few emission lines, and the need for enough data points in X to measure the curvature adequately. The effective center of each bin depends on the distribution of spectral lines within it. The bin center is calculated with a centroid in X :

$$\overline{X} = \frac{\sum x_i c_i}{\sum c_i}$$

where x_i are the diode numbers and c_i the corresponding count rates.

To simplify template fitting, each Y cross-section is normalized to its peak. Only two template widths are necessary to accomodate all the aperture sizes, because for apertures one arcsec and smaller the FWHM is determined by the 1.43 arcsec (200 micron) diode height. The remaing three apertures are 2 arcsec wide in the Y-direction, producing 280 micron cross-sections. A quadratic fit is made to the three points at the peak of the correlation curve to determine the center of the spectrum. The algorithm is the same as that used to determine the line centers in the FOS wavelength calibration.

This method produces satisfactory results when the number of counts in the peak of the cross-section is greater than 200. Results for bins with fewer than this number of counts are not included in the Y-center plots. This is particularly important for the low resolution and prism dispersers where the spectrum is confined to a small portion of the diode array.

ii. Centroiding

The centroiding method is simpler and computationally faster than cross-correlation, but has two major drawbacks: 1) the Y-center is easily thrown off by noise due to poor counting statistics in the cross-section, and 2) centroiding produces incorrect results when a Y-map is truncated, which is often the case in the existing calibration data. A cross-section consists of a set of Y-positions y_i and the corresponding count rates c_i . The centroid in Y is then $\overline{Y} = \frac{\sum y_i c_i}{\sum c_i}$.

The truncation problem can usually be alleviated by centroiding only those data points which are above the half-maximum of the cross-section. The Y-maps are rarely tuncated more than this. There is no correction for the errors produced by poor counting statistics in Y-cross sections, so this method is not considered suitable for general use.

iii. Contour Averaging

Contour averaging in effect computes the Y-positions of the upper and lower edges of the spectrum, then averages them to find the center. In this method, the contour lines at intensities of .2, .4, .6 and .8 are computed for a Y-map where each Y cross- section has been normalized to its peak. The contours for a continuum spectrum are shown in Figure 7. The average of the Y-positions of matching contour lines gives the center of the spectrum in Y along the diode array. Increasing the number of contours in the average does not result in more accurate Y-centers, because the additional contours are interpolated between the same data points in the cross-section.

Contour averaging, uses only the data in two or three Y-steps at the upper and lower edges of the spectrum. The cross-correlation method is also influenced mainly by the points at the edges of the spectrum, because that is where the difference between the template and the spectrum cross-section is greatest. Thus, the two methods are quite similar for high signal-to-noise data. Indeed, the two methods agree to within 2 microns (one-eighth the Y-step size), which is a remarkably good agreement considering the 200 micron resolution of the Y-maps. The main drawback to contour averaging is that it does not work well on noisy cross-sections, because linear interpolation is used to calculate the contours, and interpolation does not produce satisfactory results on non-monotonic functions. Therefore, cross-correlation is preferred over the contouring technique, since cross-correlation gives more precise results with low count-rate data.

C. Y-base and Theta-Z Measurements

Numerous Y-base and theta-Z measurements were made during the vacuum calibration of July 1984 and the ambient calibrations of June and August 1984. The vacuum Y-maps were made with the Pt-Cr-Ne emission line lamp, while the ambient Y-maps use the Tungsten and Deuterium external continuum lamps. The spectra were corrected for paired pulse effects with the constants $t_1 = -0.17 \times 10^{-6}$ and $t_2 = 10.5 \times 10^{-6}$ seconds. All Y-base measurements taken since the removal and replacement of the Digicons in the spring of 1984 are summarized in Table 2. The range referred to in this table is the total variation in Y-center across the diode array, which is affected both by theta-Z and the amount of distortion. The FOS file-name listed in sixth column consists of a three letter tape designation followed by the number of the file. Files on a given tape are numbered consecutively, e.g. file YAA0001 is the first file on tape YAA. Not all consecutive files were recorded without filter-grating wheel movement. The scatter in the Y-base values due to the filter-grating wheel repeatability is discussed by Hartig, Bohlin and Harms in CAL/FOS-012 and by Hartig in CAL/FOS-017.

The value of theta-Z is highly dependent on where the endpoints of the spectrum are chosen for the low dispersion modes with short spectra, and for high dispersion modes with partial coverage (H19, H78 Red and H13, H57 Blue). For example, on H57 blue, the theta-Z derived from the first 200 diodes is $-0.^\circ043$ compared with $+0.^\circ035$ if fainter spectral lines out to diode 350 are used. However, the calculated Y-bases differed by only three microns. Because the faint lines are not detected in short exposures, the endpoint of the spectrum was set at diode 200. The typical error in the determination of theta-Z is .01 degrees, for gratings that utlilize the entire diode array, and .05 degrees where theta-Z is calculated from fewer data points. The Y-base values are accurate to better than 5 microns in all cases. Since the Y-base depends on where the endpoints are chosen, the endpoints of the spectra used to compute theta-Z are listed in Table 1. Exposure time may also affect the measured value of theta-Z. Underexposure may result in the loss of fainter spectral lines at the ends of a spectrum. To avoid this, we recommend using the optimum exposure times for the 0.1 arcsec aperture listed in Table 1.

D. Shifts due to Changes in Temperature and Digicon Voltage

The Y-base and theta-Z measurements were examined to investigate whether systematic shifts occurred between data taken at different temperatures. There are three tempeatures to be considered: cold operate in vacuum at -30C, hot operate in vacuum at -10C, and ambient calibration at 20C. All observations at a given temperature were averaged in this analysis. On the red tube, there was no systematic shift in Y-base due to temperature: the mean Y-base shift between cold operate and ambient was -17 microns with a standard deviation of 34 microns. However, the red tube did show a systematic change in theta-Z of $.053 \pm .012$ degrees between cold operate and ambient. The blue tube showed a systematic shift in Y-base of -61 ± 31 microns between cold operate and ambient, but the blue side theta-Z did not show a systematic shift: the mean was shift $-.004 \pm .026$ degrees. The offsets due to changes in temperature are listed in Tables 3 and 4.

During the July vacuum calibration and the August ambient calibration the blue and red Digicons were operated at 23 and 21kV, respectively. However, in the June ambient calibration, data was obtained at 18kV for both detectors. Both detectors showed systematic decreases in Y-base values with increased voltage. The mean Y-base shift for the red tube between the June and August calibrations was -40 ± 10 microns. The blue tube Y-base measurements from June are only available on tape for gratings H40, H57, and L65. This data was supplemented by Y-base values calculated in FOS Calibration Notebook 3 for gratings H19, H27 and the prism. The mean shift for these six dispersers is -123 ± 14 microns. When Y-base values from the FOS notebook are compared to those calculated from the data tapes by the method discussed here, the results agree to within 5 microns. Theta-Z did not shift systematically with voltage on the red tube: the mean shift was $.007 \pm .009$ degrees. Theta-Z comparisons between 18 and 23kV are available for only two gratings on the blue tube. The shift on H40 was $-.032$ degrees, and $-.052$ degrees on H57. Theta-Z comparisons were made using only those gratings with full spectral coverage. The offsets due to changes in voltage are shown in Tables 5 and 6.

E. Mean Point Source Cross-Section

The main interest in FOS photometric precision is for stellar point sources, which are adequately approximated by the fully illuminated 0.1 arcsec aperture. The mean cross-section of an FOS spectrum taken with the 0.1 arcsec aperture was computed by averaging ten cross-sections from one spectrum on each detector. Each cross-section is the sum of the counts in a 50-diode bin. The cross-sections were normalized to their peaks, and then interpolated on a one micron grid. The center of each cross-section was determined by cross-correlation, and the interpolated cross-sections were then centered and summed to produce the mean curve. The H78 Y-map in file YAY0040 was chosen for the red tube cross-section because it was one of the few that was not truncated, and yet had sufficient counts for one percent accuracy. The H40 Y-map in file YAX0501 was used for the blue tube cross-section. The FWHM is 206.0 Y-base units (equivalent to microns to within 10%) for the blue curve and 206.3 Y-base units for the red curve. The mean cross-sections are tabulated in Tables 7 and 8, and plotted in Figures 8 and 9, where Y-base units and microns are used interchangably, even though Y-base units are only approximately equivalent to microns.

F. Mean Reduced Locus of Y-centers.

The average Y-center as a function of diode number in an FOS spectrum was determined for each detector. The effect of the different orientation (theta-Z) of each grating was removed by computing the deviation of the Y-center from the best fit line for each grating. The results for the three fully covered gratings on each side (Blue–H19, H27, H40; Red–H27, H40, H57) were shifted to zero Y-base and averaged to obtain the final curves, illustrated in Figures 10 and 11, and listed in Table 9.

III. Photometric Consequences of Positioning Errors (Observed)

The photometric consequences of positioning errors must be investigated separately for each combination of detector, grating, and aperture, because theta-Z is different for each grating. Because the locus of Y-centers is not symmetric in Y, a positive Y-base error has a different effect than a negative Y-base error of the same magnitude.

Ideally, we would like to directly measure the light loss, from ground based calibration data obtained in vacuum. Unfortunately, the existing internal Pt-Cr-Ne emission line spectra in Y-maps simply do not have enough counts to determine the light loss to better than 3–5% . A typical light loss curve derived from an emission line spectrum is shown in Figure 12, illustrating that the curves are noisy and of little use.

Some of the continuum spectra taken in ambient calibrations have adequate counting statistics, but because theta-Z changes with temperature, the ambient light loss curves can not be used to predict the performance of the FOS in vacuum. However, the next section will predict light loss curves from the mean locus of Y-centers, the mean spectrum cross-section,and the Y-base and theta-Z values measured in vacuum.

Light-loss curves obtained from ambient continuum spectra can be used to check whether the calculated light loss agrees with the observations. The raw data for the light loss measurements are the same Y-maps used for the Y-base measurements. The Y-maps are summed in 50 diode bins, to improve counting statistics. The spectrum at the nominal Y-base is linearly interpolated between the Y-steps of the Y-map, where necessary. Similarly, the spectra at offsets of 30, 50, 70, 80, and 90 microns above and below the nominal Y-base are also interpolated. Each light-loss curve at a given offset is simply the binned spectrum at the offset divided by the binned spectrum at the nominal Y-base. Examples of these observed light loss curves are presented in Figures 13-15.

IV. Photometric Consequenses of Positioning Errors (Modeled)

T.B.S.

TABLE 1. END POINTS, X-CENTERS AND EXPOSURE TIMES FOR FOS SPECTRA

GRATING	ENDPOINTS (DIODE)		RED DETECTOR CENTER (DIODE)	EXPOSURE TIME PER Y-STEP (S)
H13	*	*	*	*
H19	1	396	198	5
H27	1	512	256	5
H40	1	512	256	1
H57	1	512	256	1
H78	54	512	283	1
L15	1	126	63	1
L65	1	214	107	1
PRI	333	497	415	0.5

GRATING	ENDPOINTS (DIODE)		BLUE DETECTOR CENTER (DIODE)	EXPOSURE TIME PER Y-STEP (S)
H13	60	512	286	10
H19	1	512	256	5
H27	1	512	256	5
H40	1	512	256	2
H57	1	206	103	5
H78	*	*	*	*
L15	318	512	415	10
L65	295	373	334	10
PRI	27	178	102	0.5

* This combination is never used

Based on the June 1985 wavelength calibration by Sirk and Bohlin.

TABLE 2. Y-BASE AND THETA-Z MEASUREMENTS

GRATING	APERTURE	Y-BASE (microns)	RANGE IN Y (microns)	THETA-Z (degrees)	FILE	MAX CTS
RED TUBE, AMBIENT, 22 JUNE 1984, TEMP=ROOM, V=18KV, TUNGSTEN LAMP						
H27	A4	315	22	-0.032	YAQ0097	1372
H27	A4U	751	24	-0.045	YAQ0098	1270
H40	A4	-1122	25	-0.023	YAQ0076	1076
H40	A4	-1122	25	-0.022	YAQ0077	1090
H40	A4U	-687	24	-0.020	YAQ0078	680
H40	A4U	-681	21	-0.014	YAQ0079	675
H40	A4U	-698	23	-0.021	YAQ0080	685
H57	A4	-1313	32	-0.052	YAQ0082	2567
H57	A4	-1313	32	-0.051	YAQ0083	551
H57	A4	-1281	27	-0.043	YAQ0090	1320
H57	A4	-1281	31	-0.049	YAQ0091	1137
H57	A4	-1296	32	-0.051	YAQ0092	1074
H57	A4	-1297	32	-0.051	YAQ0093	1072
H57	A4U	-863	31	-0.049	YAQ0094	1011
H57	B2	-1105	31	-0.050	YAQ0107	5876
H78	A4U	626	21	0.006	YAQ0087	1376
H78	A4	186	21	0.006	YAQ0088	2262
H78	A4	186	20	0.004	YAQ0089	1125
L65	A4	-361	37	0.23	YAQ0099	23350
L65	A4	-360	37	0.24	YAQ0100	4790
L65	A4	-359	37	0.23	YAQ0101	4680
L65	A4U	77	37	0.24	YAQ0102	2930
PRI	A4	-372	5	-0.12	YAQ0104	55158
PRI	A4U	71	7	-0.15	YAQ0105	33629
BLUE TUBE, AMBIENT, 22 JUNE 1984, TEMP=ROOM, V=18KV, TUNGSTEN LAMP						
H40	A2	544	31	0.086	YAR0022	1349
H57	A4	585	10	0.039	YAR0023	597
L65	A4	-203	26	0.21	YAR0024	1172
BLUE TUBE, VACUUM, 11 JULY 1984, TEMP=-30C, V=23KV, PLATINUM LAMP						
H13	A4	-249	13	-0.037	YAT1896	1427
H13	A4	-249	15	-0.039	YAT1897	1437
H13	A4	-261	17	-0.044	YAT1898	1953

TABLE 2, CONTINUED

GRATING	APERTURE	Y-BASE (microns)	RANGE IN Y (microns)	THETA-Z (degrees)	FILE	MAX CTS
BLUE TUBE, VACUUM, 11 JULY 1984, TEMP=-30C, V=23KV, PLATINUM LAMP						
H19	A4	-536	19	0.088	YAT1876	87
H19	A4	-538	22	0.10	YAT1877	89
H19	A4	-537	24	0.11	YAT1878	75
H27	A4	-981	25	0.064	YAT1874	553
H27	A4	-972	25	0.060	YAT1875	527
H40	A4	520	16	0.043	YAT1872	1732
H40	A4	514	19	0.055	YAT1873	1994
H57	A4	556	17	-0.044	YAT1899	1953
L65	A4	-314	24	0.14	YAT1884	1208
L65	A4	-319	34	0.20	YAT1885	1235
L65	A4	-319	29	0.17	YAT1886	1160
L65	A4	-267	25	0.15	YAT1890	1203
L65	A4	-283	29	0.18	YAT1894	1182
PRI	A4	-390	6	-0.11	YAT1887	1774
PRI	A4	-393	5	-0.09	YAT1888	2023
PRI	A4	-341	2	-0.01	YAT1892	2061
PRI	A4	-351	3	-0.06	YAT1895	2166
RED TUBE, VACUUM, 15 JULY 1984, TEMP=-30C, V=21KV, PLATINUM LAMP						
H19	A4	-218	33	-0.077	YAX0020	2854
H19	A4U	216	35	-0.083	YAX0021	2405
H27	A4	316	48	-0.11	YAX0022	10950
H40	A4	-1112	36	-0.082	YAX0025	6948
H57	A4	-1207	45	-0.10	YAX0028	31335
H78	A4U	567	18	-0.058	YAX0029	14333
L15	A4	-121	9	-0.10	YAX0030	400
BLUE TUBE, VACUUM, 17 JULY 1984, TEMP=-10C, V=23kV, PLATINUM LAMP						
H13	A4U	+214	19	-0.040	YAX0467	7300
H19	A4	-514	28	0.070	YAX0474	3500
H19	A4	-499	28	0.064	YAX0488	80
H19	A2	-501	25	0.067	YAX0486	2500
H19	C1	-501	25	0.063	YAX0489	7000

TABLE 2, CONTINUED

GRATING	APERTURE	Y-BASE (microns)	RANGE IN Y (microns)	THETA-Z (degrees)	FILE	MAX CTS
BLUE TUBE, VACUUM, 17 JULY 1984, TEMP=-10C, V=23kV, PLATINUM LAMP						
H19	B2	-289	25	0.067	YAX0481	2097
H19	B3	-287	25	0.066	YAX0482	6209
H19	A2	-501	26	0.065	YAX0486	2602
H19	A3	-502	32	0.074	YAX0487	1995
H19	C1	-501	24	0.063	YAX0489	7027
H19	C2	-300	27	0.065	YAX0490	3743
H27	A4	-985	22	0.050	YAX0473	13000
H40	A4	507	16	0.037	YAX0476	25000
H40	A4	500	15	0.034	YAX0500	4007
H40	A4U	923	16	0.037	YAX0499	4152
H40	C1	499	15	0.038	YAX0496	31903
H40	C1	499	14	0.037	YAX0497	31994
H40	C1	920	14	0.036	YAX0498	31684
H40	A3	497	15	0.040	YAX0501	14087
H40	A3U	916	15	0.036	YAX0502	13928
H40	A2U	920	15	0.037	YAX0503	10385
H40	A2	503	15	0.039	YAX0504	10438
H40	B3	714	15	0.038	YAX0505	28848
H40	B2	711	16	0.042	YAX0506	9882
H40	B1	714	15	0.039	YAX0507	9719
H57	A4	515	9	-0.043	YAX0478	20000
L15	A4U	+6	2	0.008	YAX0469	2000
L65	A4	-274	21	0.22	YAX0471	24000
RED TUBE, VACUUM, 17 JULY 1984, TEMP=-10C, V=21KV, PLATINUM LAMP						
H19	A4	-212	32	-.073	YAX0522	2600
H27	A4	+342	42	-.094	YAX0523	30000

TABLE 2, CONTINUED

GRATING	APERTURE	Y-BASE (microns)	RANGE IN Y (microns)	THETA-Z (degrees)	FILE	MAX CTS
BLUE TUBE, VACUUM, 20 JULY 1984, TEMP=-10C, V=23KV, PLATINUM LAMP						
H13	A4	-222	16	-0.094	YAX0902	274
H13	A4U	201	18	-0.11	YAX0903	324
H13	A4	-234	20	-0.12	YAX0920	246
H13	A4U	184	13	-0.081	YAX0921	271
RED TUBE, VACUUM, 20 JULY 1984, TEMP=-10C, V=21KV, PLATINUM LAMP						
H78	A4	151	37	-0.12	YAX0907	9898
H78	A4	169	25	-0.078	YAX0908	9338
H78	A4U	606	22	-0.072	YAX0909	6698
RED TUBE, AMBIENT, 20-21 AUGUST 1984, TEMP=ROOM, V=21kV, TUNGSTEN LAMP						
H19	C1	-260	33	-0.044	YAY0064	323
H19	C3	-40	27	-0.032	YAY0062	643
H19	B3	-57	26	-0.035	YAY0065	248
H27	A4	289	32	-0.056	YAY0047	351
H27	A4U	714	30	-0.052	YAY0036	250
H27	A2	290	32	-0.056	YAY0045	6181
H27	A3	290	32	-0.057	YAY0046	1460
H27	B1	489	31	-0.054	YAY0048	4798
H27	B2	492	30	-0.052	YAY0049	1673
H27	B3	491	31	-0.056	YAY0050	9854
H27	C1	288	33	-0.059	YAY0052	12616
H27	C2	506	31	-0.058	YAY0053	9000
H27	C3	510	29	-0.054	YAY0054	24039
H27	C4	502	34	-0.062	YAY0055	20610
H40	A4	-1099	20	-0.020	YAY0037	4500
H57	A4	-1265	32	-0.048	YAY0039	10000
H78	A4	140	23	0.002	YAY0058	11068
H78	A4U	593	23	0.007	YAY0040	7000
H78	A2	140	22	0.002	YAY0056	54946
H78	A3	142	22	0.002	YAY0057	29262
H78	B1	342	21	0.003	YAY0059	41557
H78	B2	344	20	0.001	YAY0060	32906
H78	C2	358	21	0.006	YAY0061	40127
L65	A4	-360	28	0.23	YAY0044	5000
PRI	A4	-317	5	-0.043	YAY0043	60000

TABLE 2, CONTINUED

GRATING	APERTURE	Y-BASE (microns)	RANGE IN Y (microns)	THETA-Z (degrees)	FILE	MAX CTS
BLUE TUBE, AMBIENT, 26 AUGUST 1984, TEMP=ROOM, V=23KV, TUNGSTEN LAMP						
H19	C1	-561	31	0.072	YAZ0106	327
H27	A3	-1057	23	0.054	YAZ0107	1128
H40	A4	412	20	0.054	YAZ0108	806
H57	A4	476	7	-0.013	YAZ0109	1130
L65	A4	-336	50	0.16	YAZ0110	2038
PRI	A4	-434	3	-0.040	YAZ0111	1720

The lower half of a paired aperture was used unless otherwise noted with a U for the upper aperture.

TABLE 3. Y-BASE OFFSETS DUE TO CHANGES IN TEMPERATURE.

Red Tube , V=21kv, 0.1 arcsec aperture

Grating	Y-base T=-30 (microns)	Y-base T=-10 (microns)	Shift between T=-30 and t=-10 (microns)	Y-base Ambient (microns)	Shift between T=-30 and ambient (microns)
H19	-218	-212	6	-261	-43
H27	316	342	26	289	-27
H40	-1112			-1099	13
H57	-1207			-1265	-52
H78U	567			593	26
					Mean: -17 +/- 34

Blue tube , V=23kv, 0.1 arcsec aperture

Grating	Y-base T=-30	Y-base T=-10	Shift between T=-30 and t=-10	Y-base Ambient	Shift between T=-30 and ambient
H19	-537	-514	23	-561	-24
H27	-977	-985	-8	-1057	-80
H40	517	507	-10	412	-105
H57	556	516	-40	477	-79
L65	-300	-274	44	-336	-36
PRI	-390			-434	-44
			Mean: 2 +/-32		Mean: -61 +/- 31

TABLE 4. THETA-Z OFFSETS DUE TO CHANGES IN TEMPERATURE.

Red Tube , V=21kv, 0.1 arcsec aperture

Grating	Theta-Z T=-30 (degrees)	Theta-Z T=-10 (degrees)	Shift between T=-30 and t=-10 (degrees)	Theta-Z Ambient (degrees)	Shift between T=-30 and ambient (degrees)
H19	-.077	-.072	.005	-.044	.033
H27	-.109	-.093	.016	-.056	.053
H40	-.082			-.020	.062
H57	-.100			-.048	.052
H78U	-.058	-.043	.015	.007	.065
					Mean: .053 +/- .012

Blue Tube , V=23kv, 0.1 arcsec aperture

Grating	Theta-Z T=-30	Theta-Z T=-10	Shift between T=-30 and t=-10	Theta-Z Ambient	Shift between T=-30 and ambient
H19	.106	.080	-.026	.072	-.034
H27	.062	.050	-.012	.055	-.007
H40	.049	.034	-.015	.054	-.005
H57	-.044	-.043	.001	-.014	.030
			Mean: .013 +/- .011		Mean: -.004 +/- .026

TABLE 5. Y-BASE OFFSETS DUE TO CHANGE IN VOLTAGE

Red Tube, ambient, 0.1 arcsec aperture

Grating	Y-base 18kv (microns)	Y-base 21kv (microns)	Shift between 18kv and 23kv
H27	315	289	-26
H27U	751	714	-37
H40	-1044	-1099	-55
H57	-1226	-1265	-39
H78	188	140	-48
H78U	627	593	-34
			Mean: -40 +/- 10

Blue Tube, ambient, 0.1 arcsec aperture

Grating	Y-base 18kv (microns)	Y-base 23kv (microns)	Shift between 18kv and 23kv
H19	-437	-561	-124
H27	-954	-1057	-103
H40	544	412	-132
H57	585	476	-109
L65	-203	-336	-133
PRI	-295	-434	-139
			Mean: -123 +/- 14

TABLE 6. THETA-Z OFFSETS DUE TO CHANGE IN VOLTAGE

Red Tube, ambient, 0.1 arcsec aperture

Grating	Theta-Z 18kv (degrees)	Theta-Z 21kv (degrees)	Shift between 18kv and 23kv
H27U	-.045	-.052	-.007
H40	-.012	-.020	-.008
H57	-.049	-.048	.001
H78	.006	.002	-.004
H78U	.006	.007	.001
			Mean: .007 +/- .009

Blue Tube, ambient, 0.1 arcsec aperture

Grating	Theta-Z 18kv (degrees)	Theta-Z 23kv (degrees)	Shift between 18kv and 23kv
H40	.086	.054	-.032
H57	.039	-.013	-.052

TABLE 7. RED TUBE MEAN POINT SOURCE CROSS-SECTION

Y (MICRONS)	INTENSITY
-150.00	4.13142E-02
-145.00	4.49599E-02
-140.00	5.01553E-02
-135.00	5.93092E-02
-130.00	7.07596E-02
-125.00	9.03191E-02
-120.00	0.13048
-115.00	0.18436
-110.00	0.27366
-105.00	0.43243
-100.00	0.60533
-95.000	0.77064
-90.000	0.86509
-85.000	0.92411
-80.000	0.96145
-75.000	0.97576
-70.000	0.98225
-65.000	0.98720
-60.000	0.99058
-55.000	0.99310
-50.000	0.99531
-45.000	0.99691
-40.000	0.99758
-35.000	0.99803
-30.000	0.99833
-25.000	0.99826
-20.000	0.99798
-15.000	0.99768
-10.000	0.99816
-5.0000	0.99905

Y (MICRONS)	INTENSITY
0.0000	1.0000
5.0000	0.99989
10.000	0.99887
15.000	0.99739
20.000	0.99590
25.000	0.99490
35.000	0.99354
40.000	0.99268
45.000	0.99170
50.000	0.99061
55.000	0.98852
60.000	0.98574
65.000	0.98217
70.000	0.97501
75.000	0.96533
80.000	0.95167
85.000	0.91036
90.000	0.83798
95.000	0.74179
100.00	0.59572
105.00	0.42942
110.00	0.27304
115.00	0.16328
120.00	0.11605
125.00	8.39821E-02
130.00	6.39523E-02
135.00	5.40057E-02
140.00	4.62675E-02
145.00	4.02842E-02
150.00	3.75334E-02

TABLE 8. BLUE TUBE MEAN POINT SOURCE CROSS-SECTION

Y (MICRONS)	INTENSITY	Y (MICRONS)	INTENSITY
-150.00	2.18572E-02	0.00000E+00	1.0000
-145.00	3.04461E-02	5.0000	1.0015
-140.00	4.27927E-02	10.000	1.0026
-135.00	5.86833E-02	15.000	1.0027
-130.00	8.58453E-02	20.000	1.0018
-125.00	0.12515	25.000	1.0008
-120.00	0.17346	30.000	1.0003
-115.00	0.25360	35.000	0.99978
-110.00	0.35651	40.000	0.99926
-105.00	0.47012	45.000	0.99859
-100.00	0.58599	50.000	0.99881
-95.000	0.69565	55.000	0.99912
-90.000	0.79401	60.000	0.99734
-85.000	0.87521	65.000	0.99160
-80.000	0.92664	70.000	0.98287
-75.000	0.95811	75.000	0.96440
-70.000	0.97718	80.000	0.92870
-65.000	0.98364	85.000	0.87436
-60.000	0.98824	90.000	0.80381
-55.000	0.99301	95.000	0.70301
-50.000	0.99483	100.00	0.58684
-45.000	0.99521	105.00	0.46980
-40.000	0.99533	110.00	0.36138
-35.000	0.99587	115.00	0.26733
-30.000	0.99640	120.00	0.18314
-25.000	0.99654	125.00	0.12813
-20.000	0.99667	130.00	9.20825E-02
-15.000	0.99705	135.00	6.49018E-02
-10.000	0.99779	140.00	4.71736E-02
-5.0000	0.99879	145.00	3.67673E-02

TABLE 9. MEAN LOCUS OF Y-CENTERS

BLUE TUBE

DIODE	Y-CENTER (MICRONS)
25.	7.5
76.	-0.9
127.	-3.4
178.	-3.4
229.	-2.2
280.	-1.4
331.	-0.3
382.	0.3
433.	1.3
484.	2.5

RED TUBE

DIODE	Y-CENTER (MICRONS)
25.	-13.3
76.	-3.3
127.	3.6
178.	7.5
229.	8.5
280.	7.5
331.	4.3
382.	0.7
433.	-3.4
484.	-10.2

FIGURE CAPTIONS

Figure 1. Y-center as a function of diode for red tube H40, ambient calibration, 21kv voltage, August 20, 1984. Crosses: the Y-center for each bin. The solid line is the least squares fit.

Figure 2. Y-center as a function of diode for red tube prism, ambient calibration, 21kv voltage, August 20, 1984. Note that the X scale is expanded to cover the region from diode 400 to 500 where the prism spectrum is located.

Figure 3. Y-center as a function of diode for blue tube H27 vacuum calibration, 23kv voltage, July 17, 1984.

Figure 4. Y-center as a function of diode for blue tube H57 vacuum calibration, 23kv voltage, July 17, 1984. The diode array is only partially covered by the spectrum because the blue tube attenuates strongly above 5500A.

Figure 5. Cross-section of the 0.1 arcsec spectrum with a bin size of 50 diodes. The size of the Y-steps is 16 microns.

Figure 6. Cross-section of an 1.0 arcsec spectrum with a bin size of 50 diodes. The profile is much more rounded than the 0.1 arcsec aperture, because the spectrum is almost as wide as the diode array.

Figure 7. A contour plot of a normalized Y-map of a continuum spectrum, clearly showing the curvature produced by the red Digicon. The contour levels are at .2, .4, .6, .8, and .95 of the peak value

Figures 8 and 9. Mean cross-sections of a point source spectrum as represented by a 0.1 arcsec aperture spectrum with the red and blue detectors. This cross-section should adequately represent the actual cross-section for a point source in any FOS aperture.

Figures 10 and 11. Mean Y-center as a function of diode for each detector. The curve has been reduced to zero theta-Z and zero Y-base.

Figure 12. The effects of error in Y-position as a function of diode number determined from an emission line spectrum on the red tube. The upper plot is for positive Y-base errors, the lower plot for negative Y-base errors. The two plots differ because the locus

of Y-centers is not symmetric. The five curves represent errors of 30 microns (solid line), 50 microns (long dash), 70 microns (medium dash), 80 microns (short dash), and 90 microns (dot-dash). The error in the curves is at the 5% level.

Figures 13–15. The effects of error in Y-position determined from continuum spectra on the red tube. The lines are coded as in Figure 12. The noise level is 1–2%, because the total counts per bin is higher than that of the emission line spectra.

Figure 1.

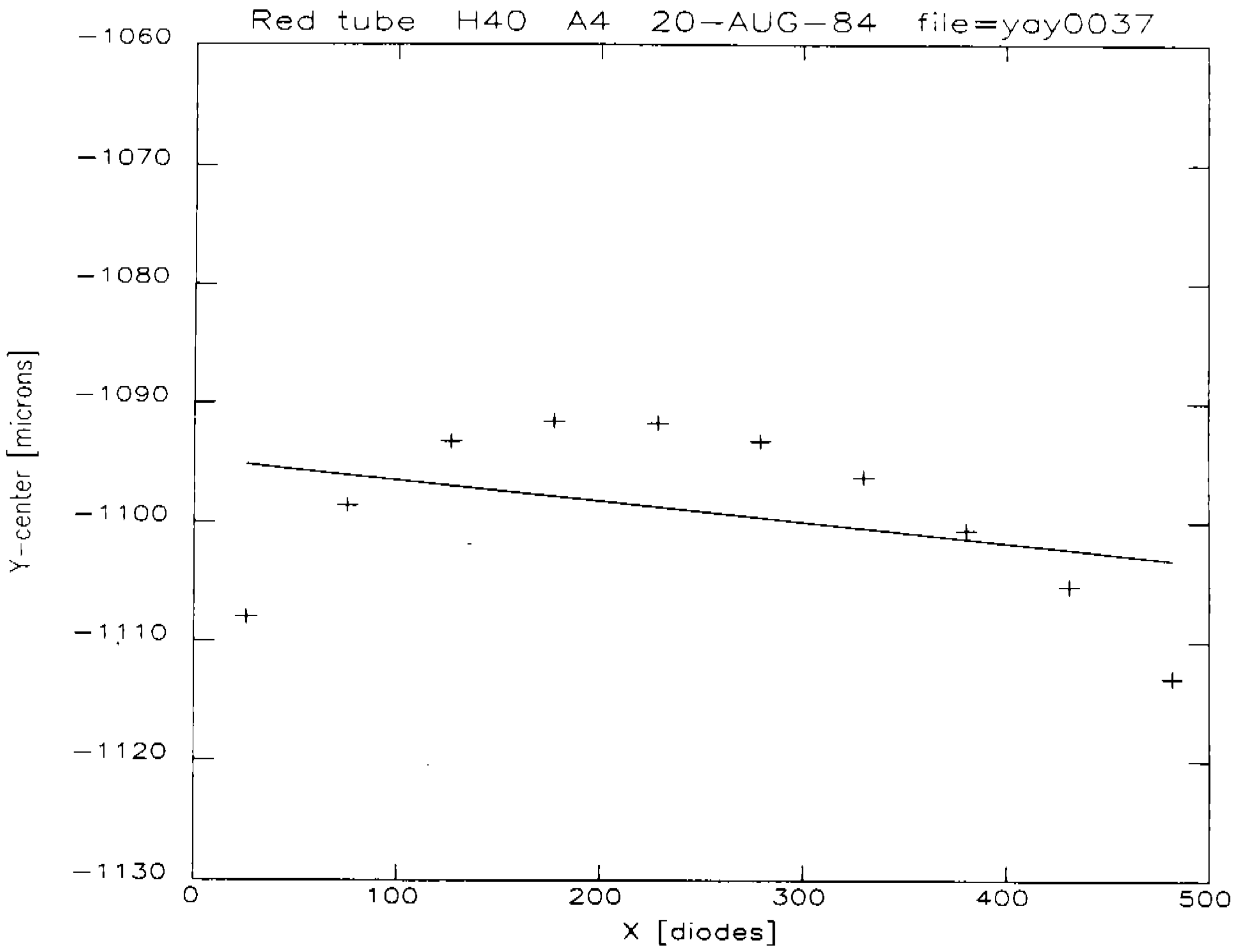

Figure 2.

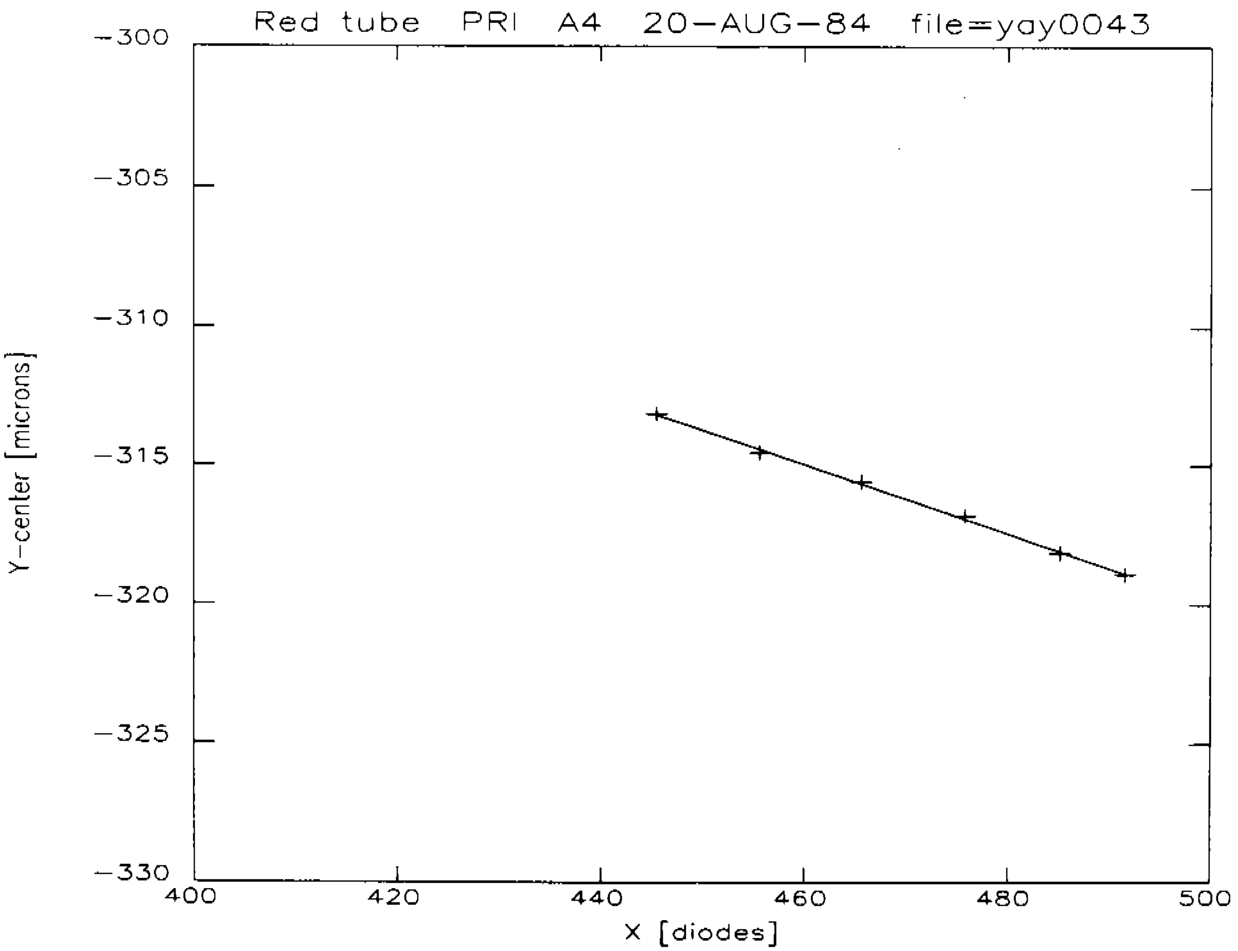

Figure 3

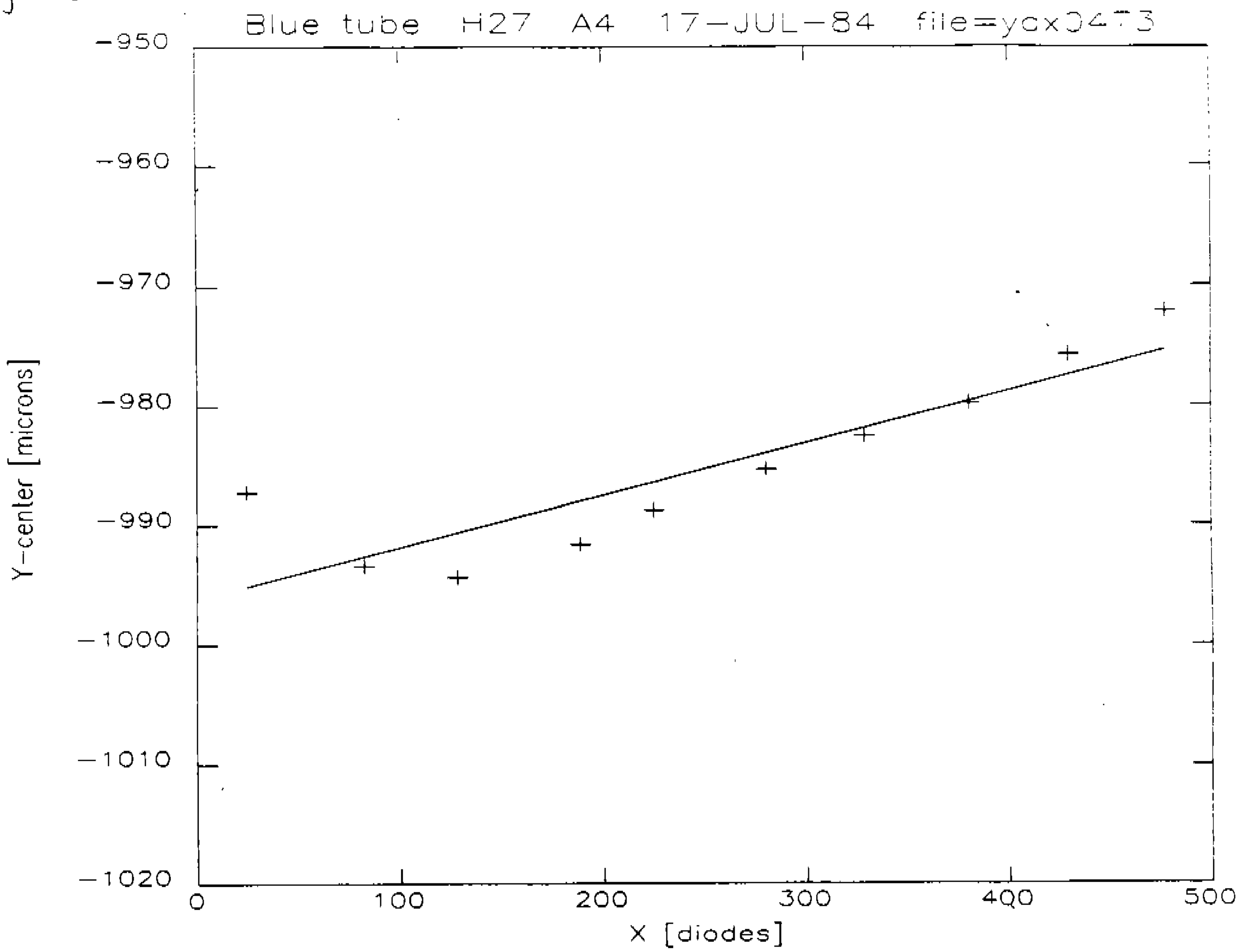

Figure 4

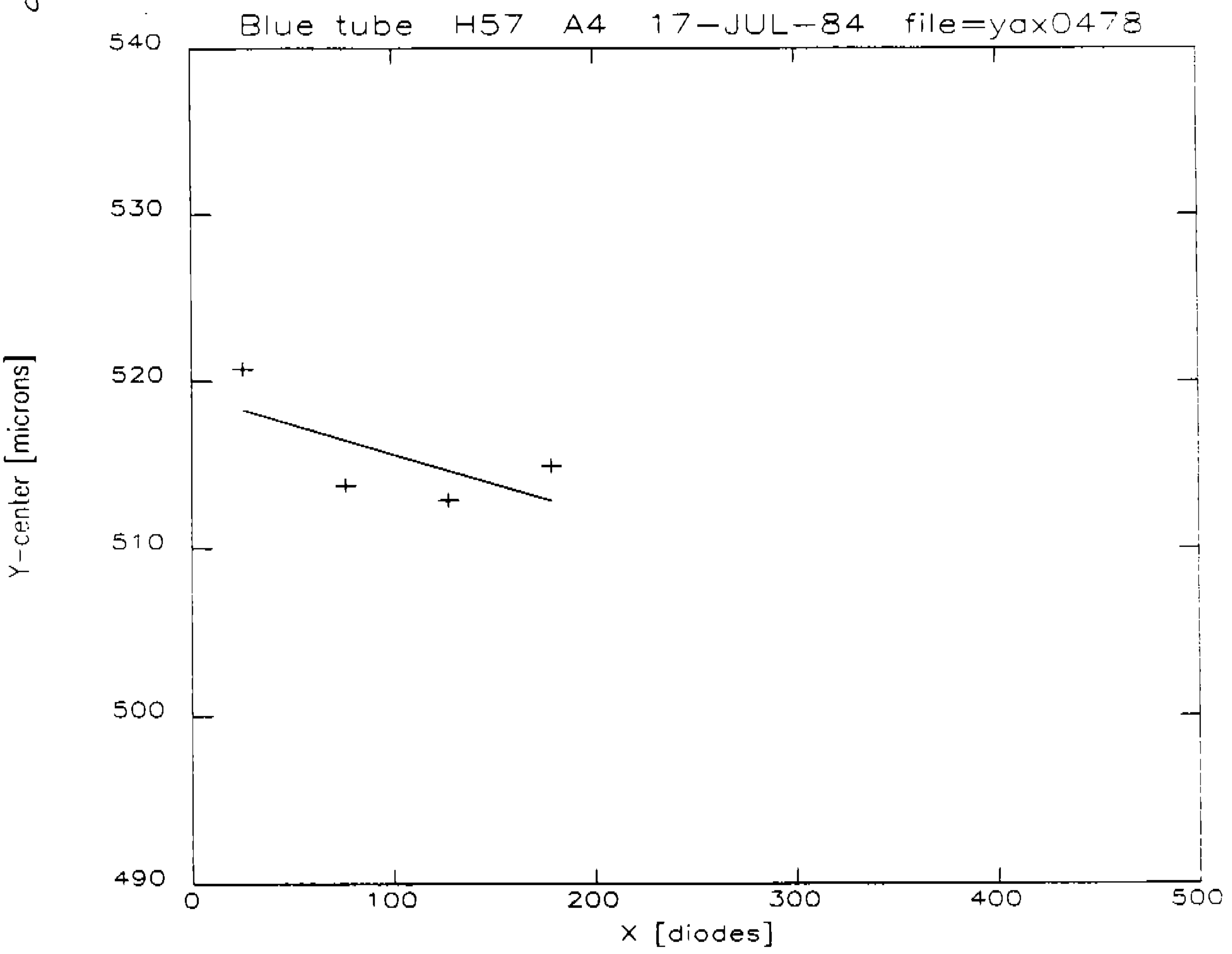

Figure 5.

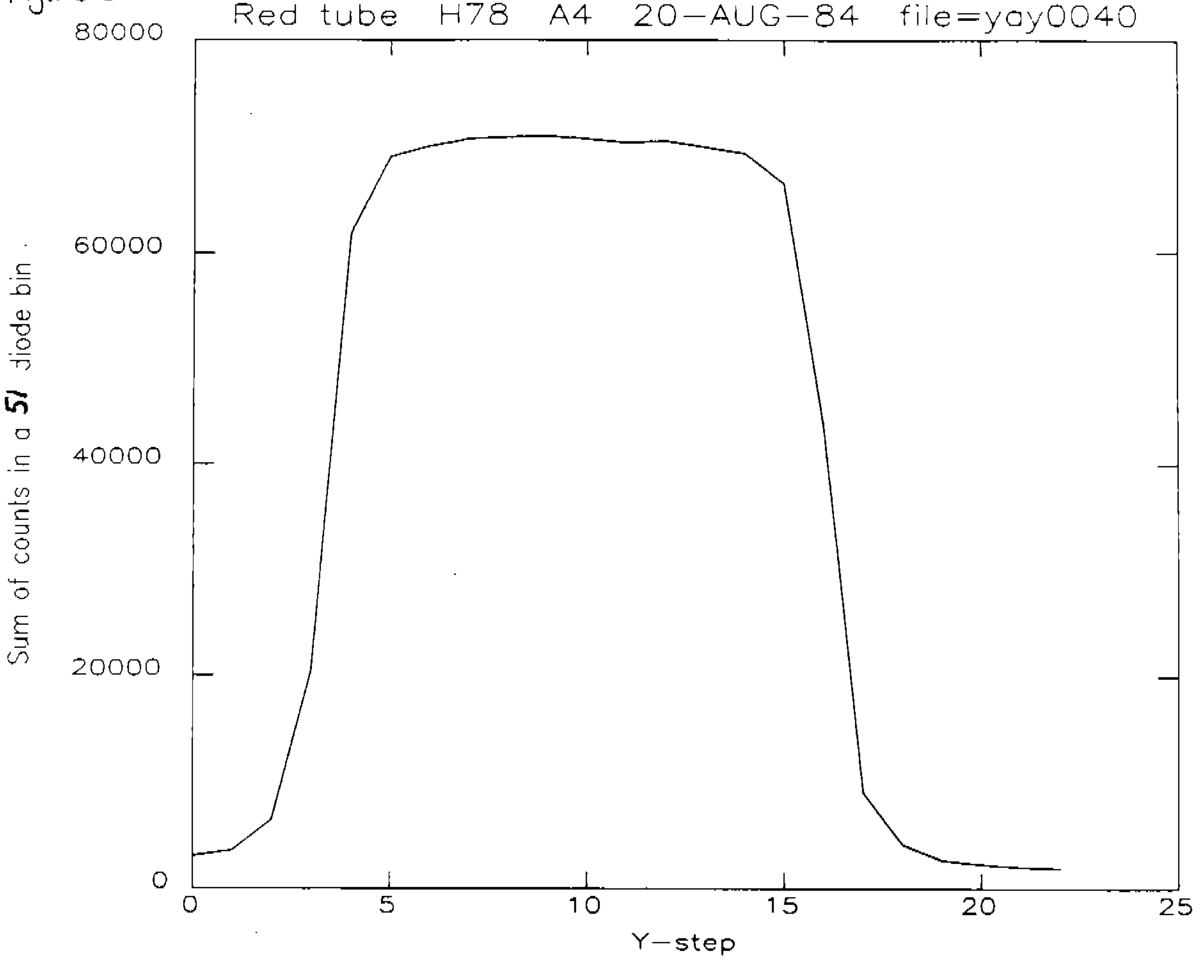

Figure 6.

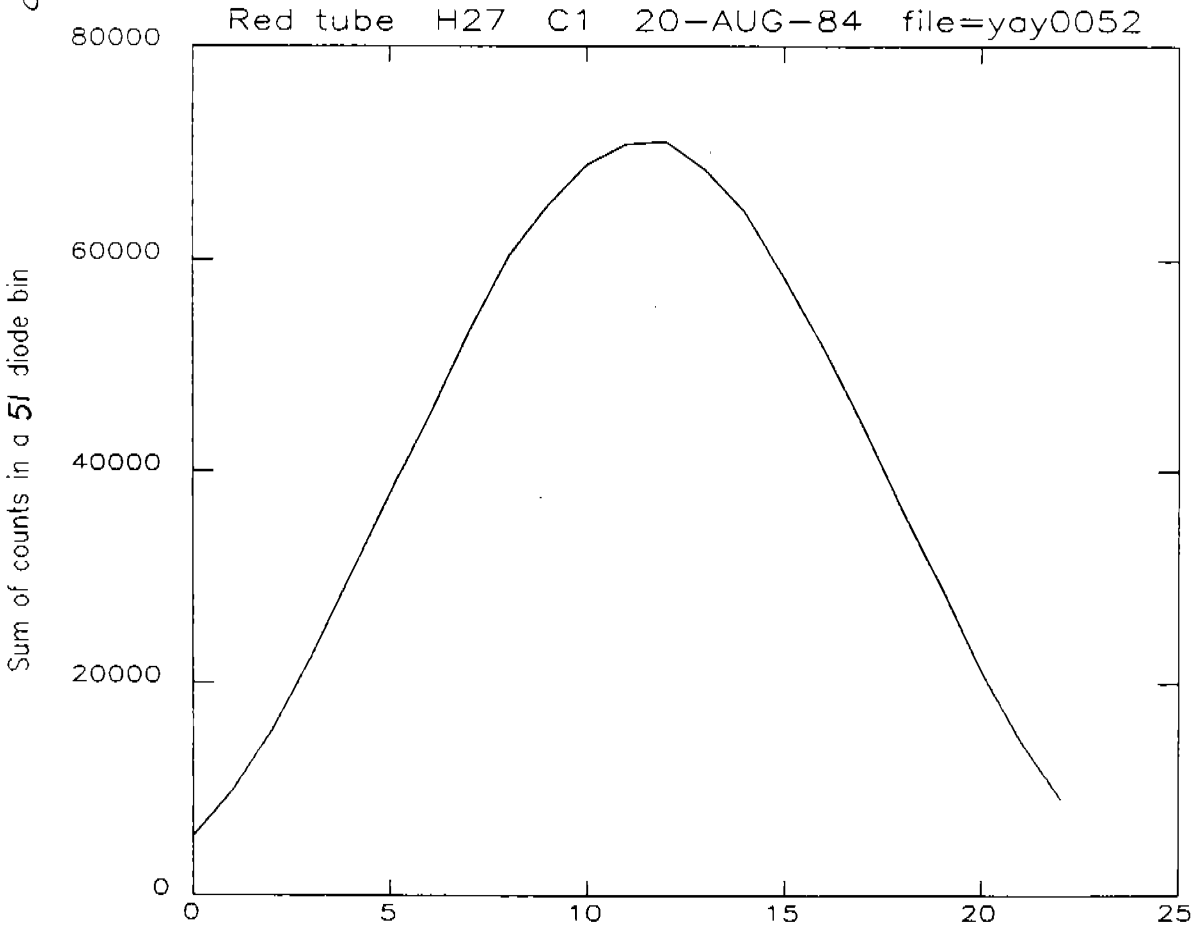

Figure

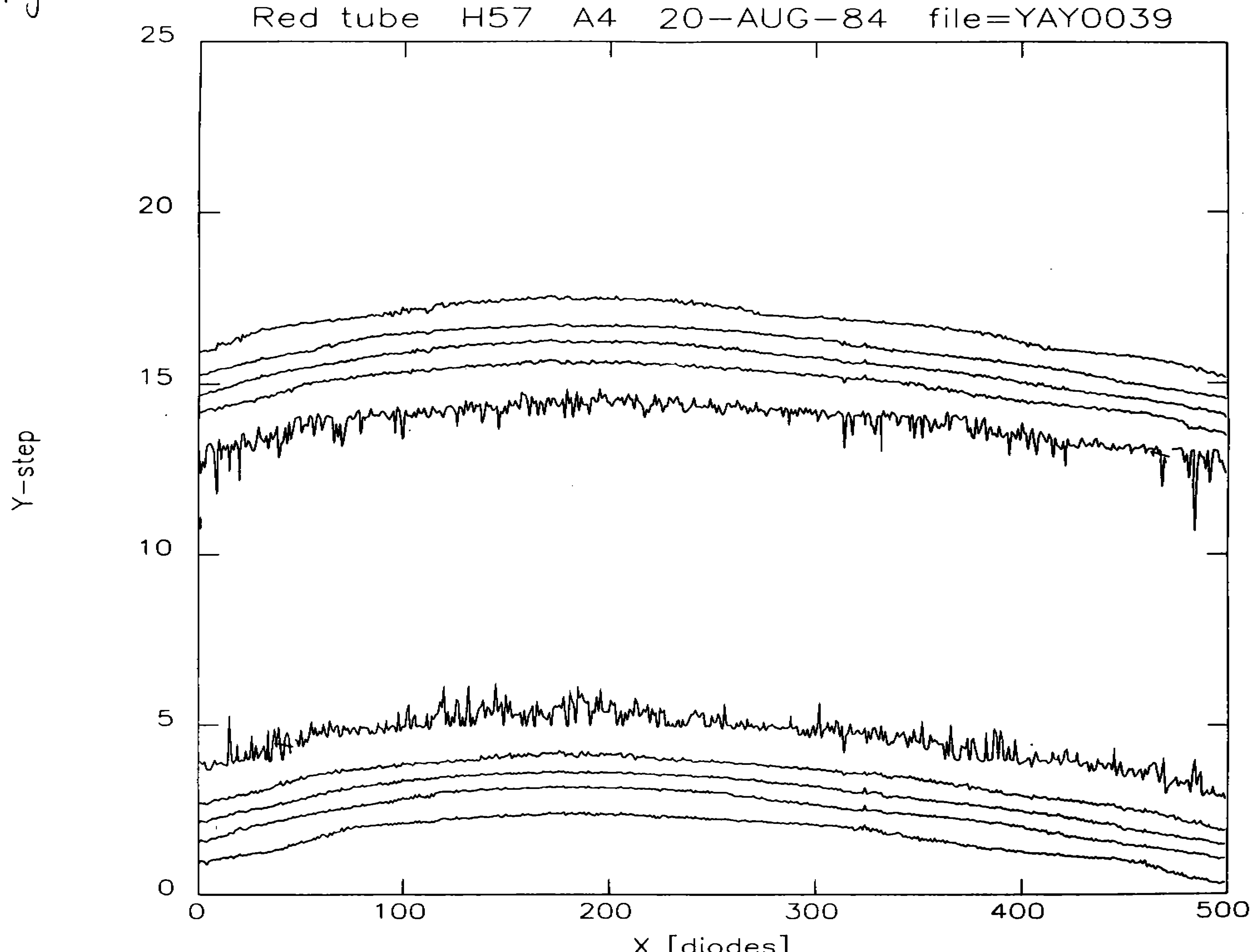

Red tube H57 A4 20-AUG-84 file=YAY0039
25
20
15
10
5
0
Y-step
0
100
200
300
400
500
X [diodes]

Figure 8.

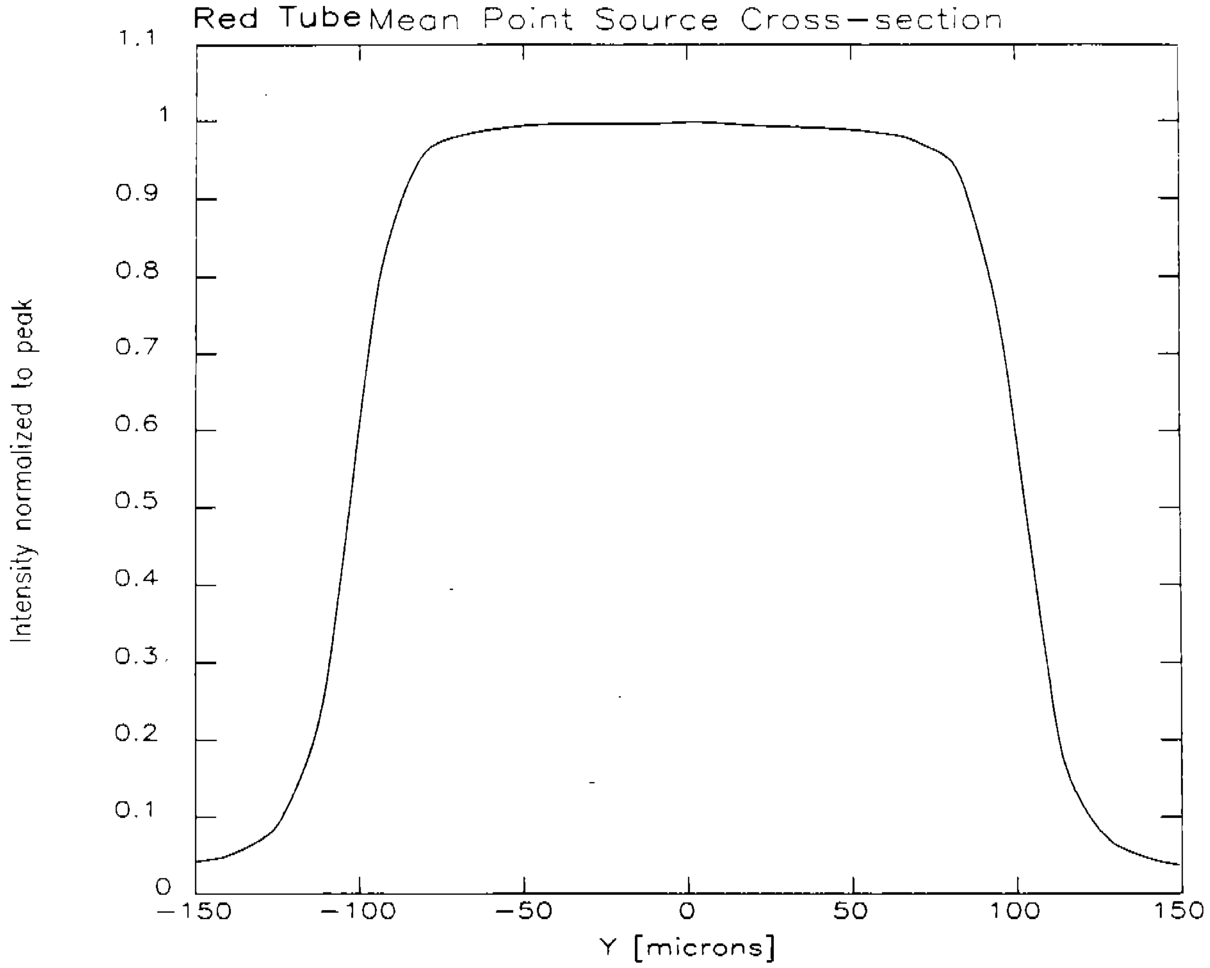

Figure 9.

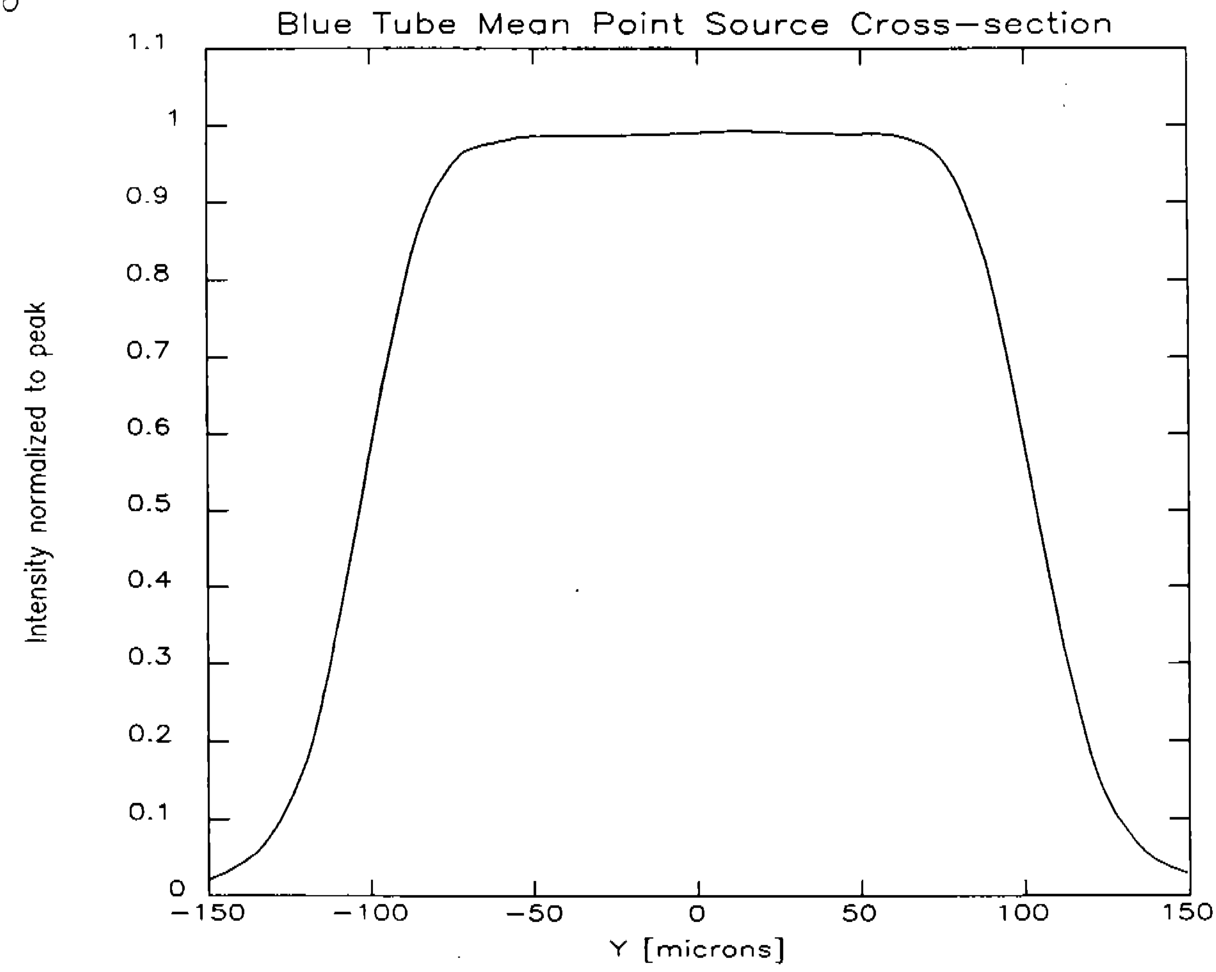

Figure 10.

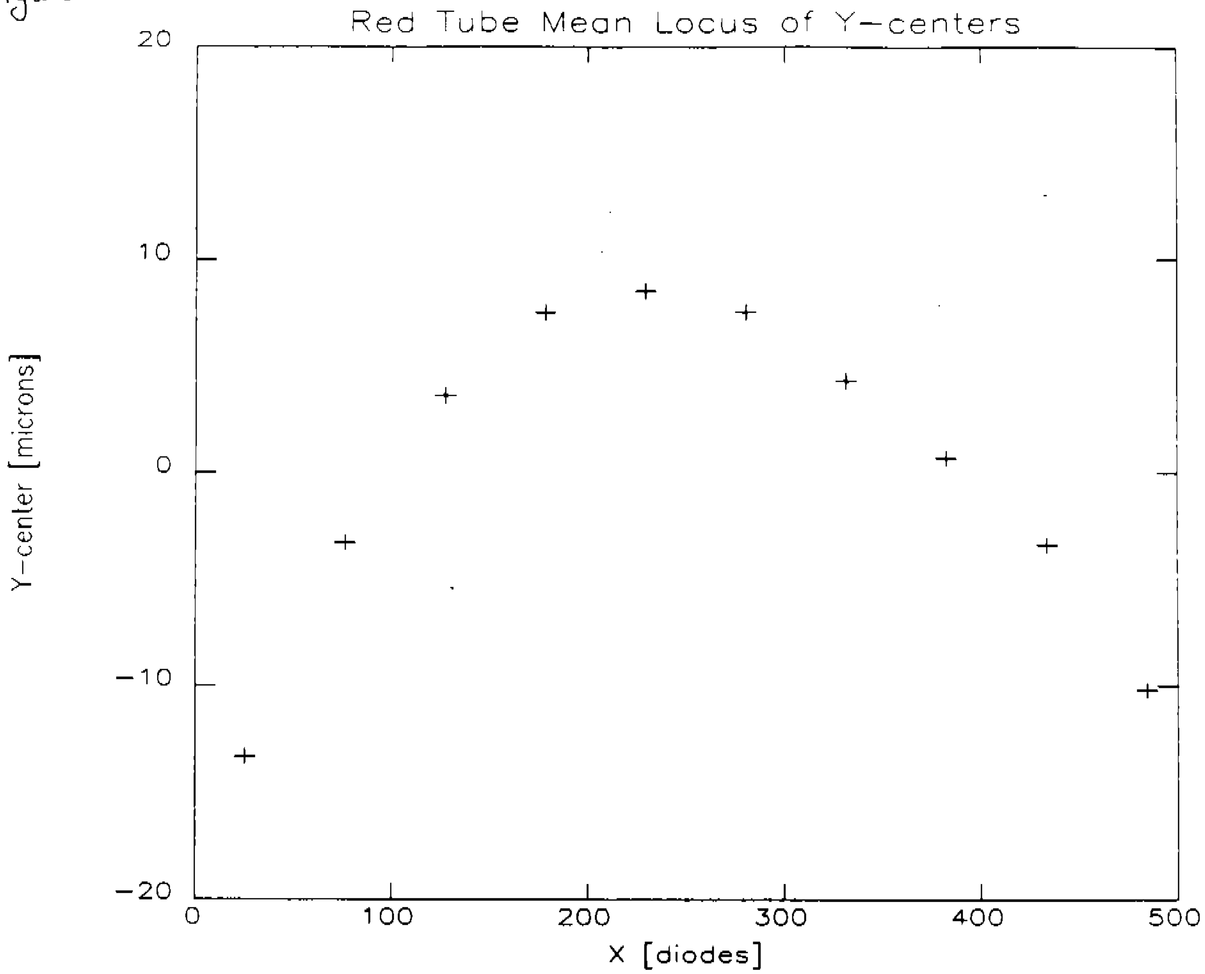

Figure 11.

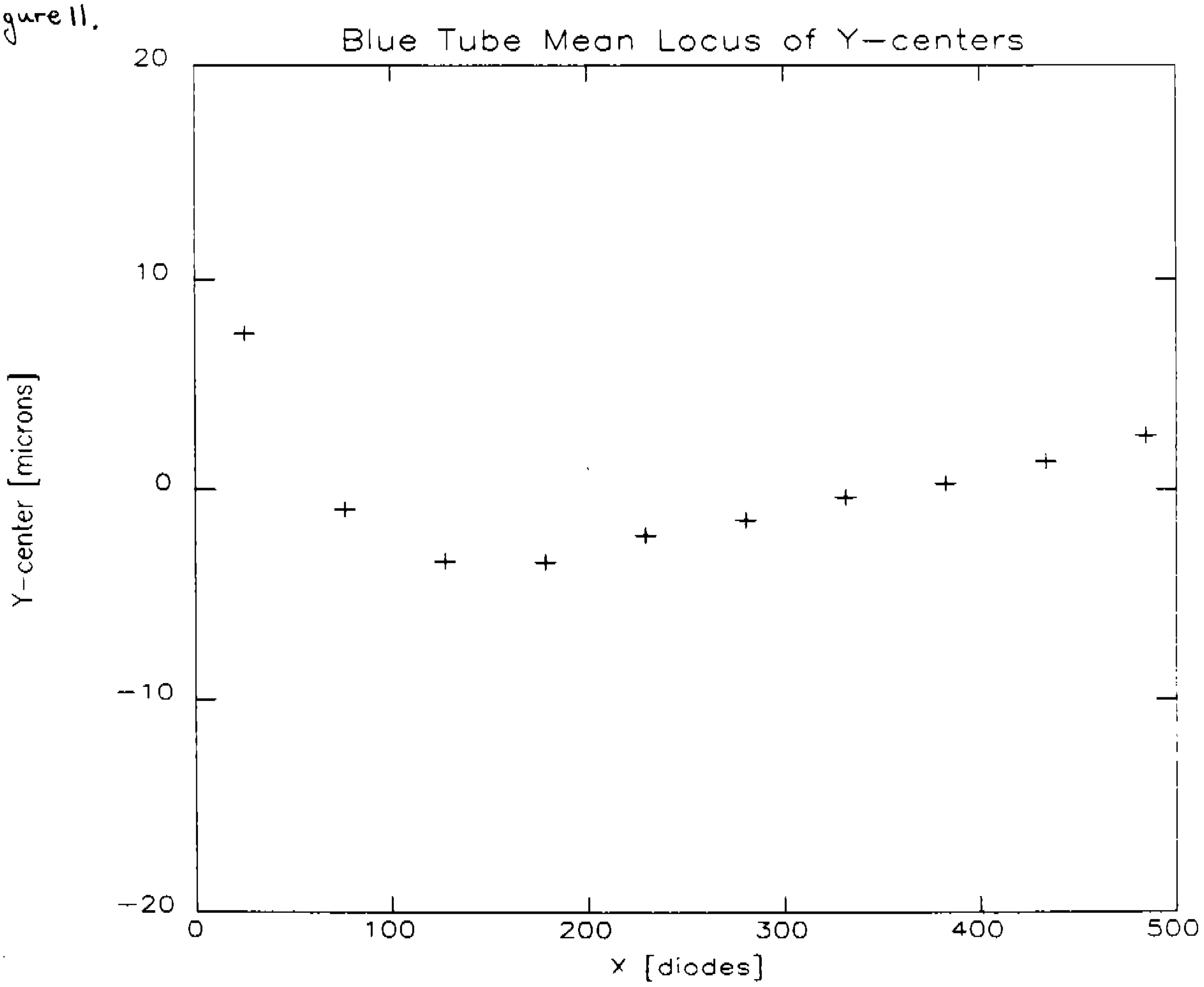

Figure 12

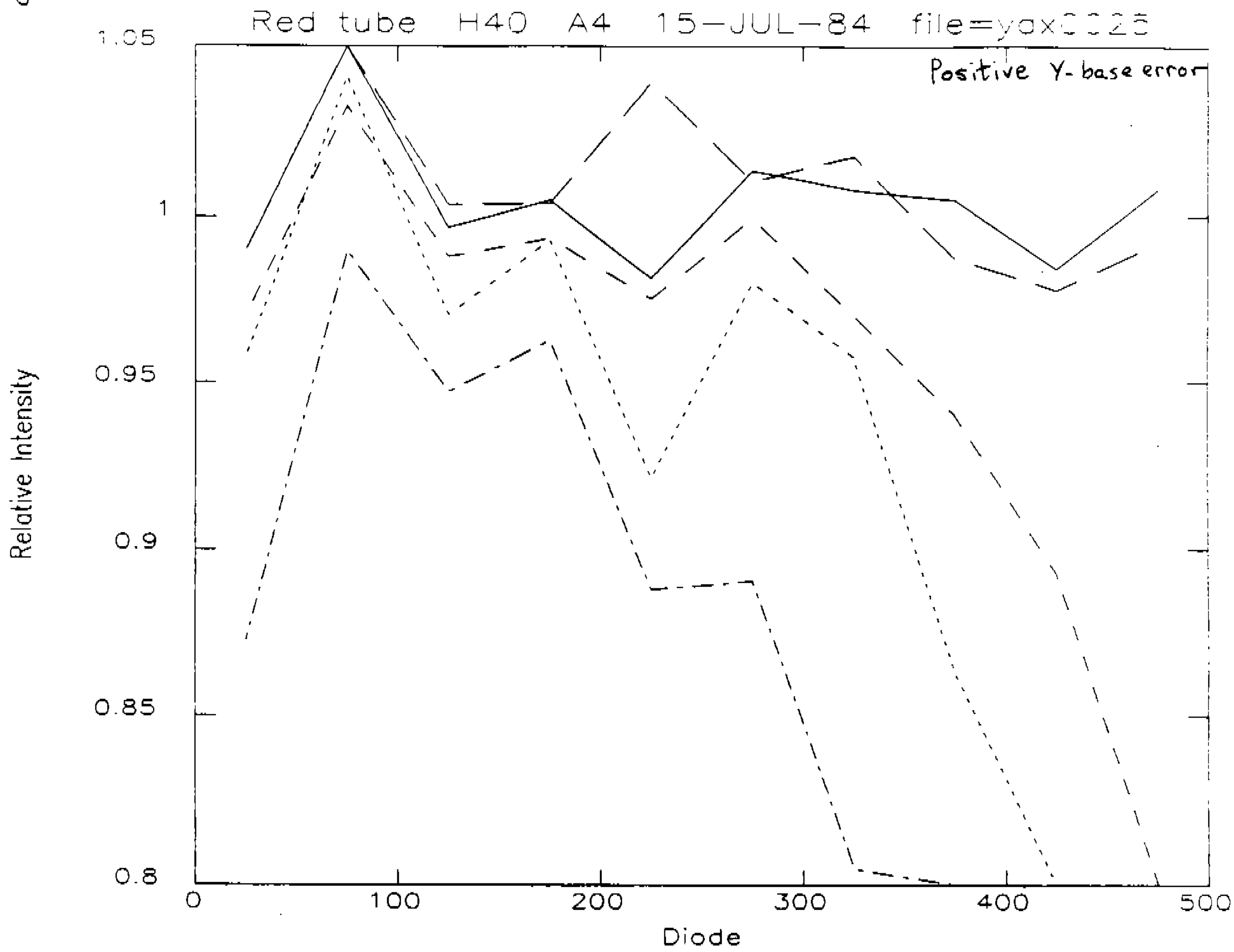
Red tube H40 A4 15-JUL-84 file=yax0025
Positive Y-base error
Relative Intensity
Diode
1.05
1
0.95
0.9
0.85
0.8
0
100
200
300
400
500

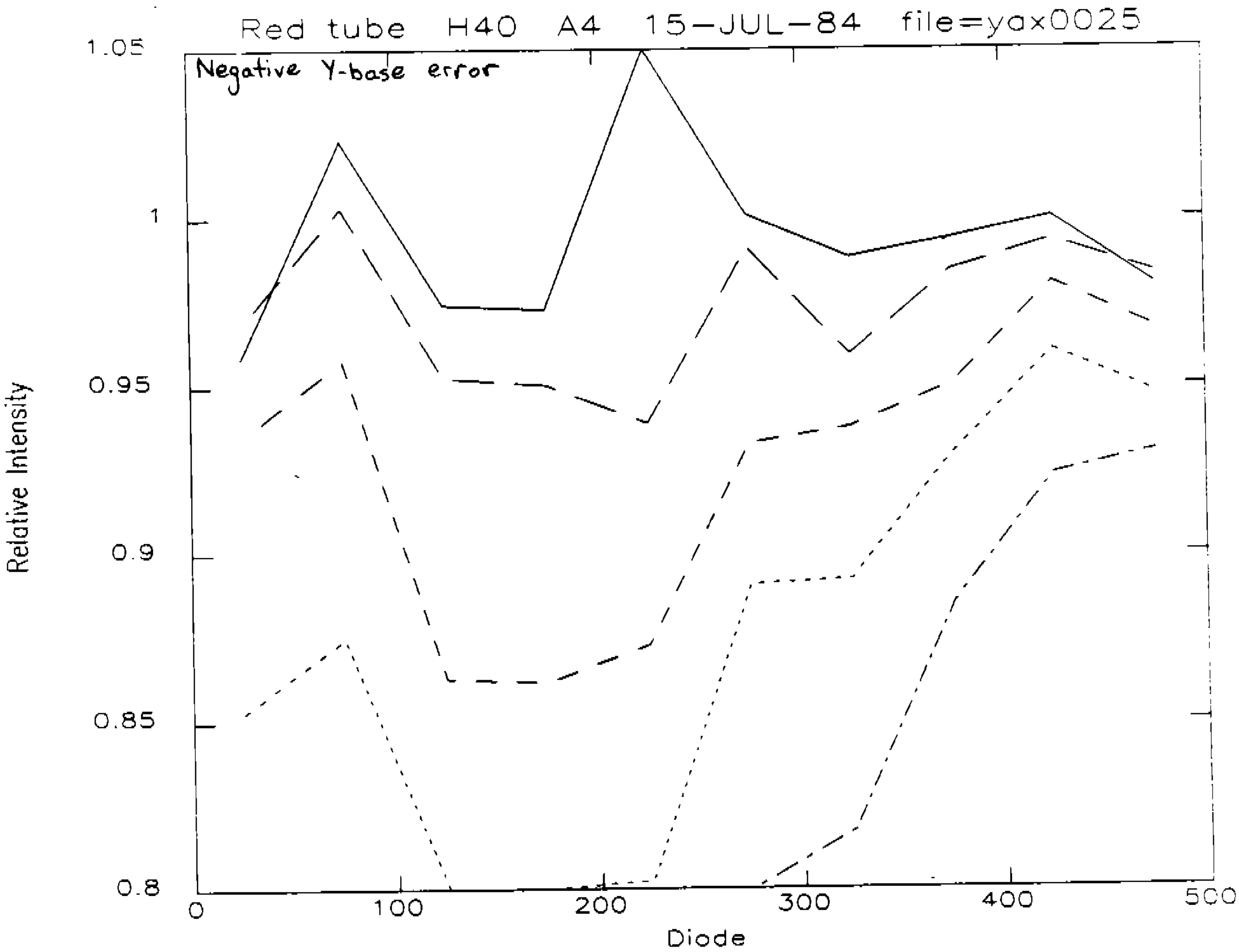
Red tube H40 A4 15-JUL-84 file=yax0025
Negative Y-base error
Relative Intensity
Diode
1.05
1
0.95
0.9
0.85
0.8
0
100
200
300
400
500

Figure 13.

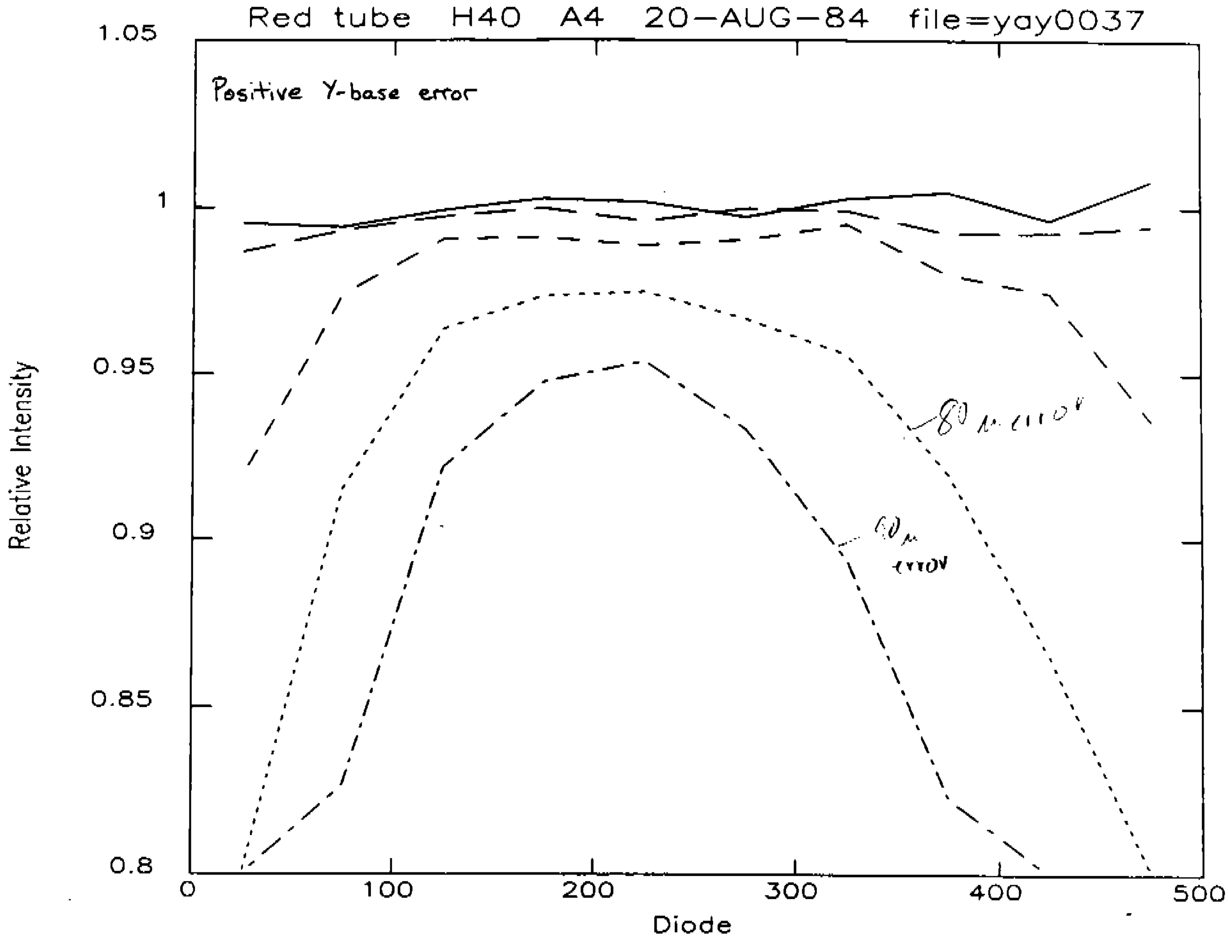
Red tube H40 A4 20–AUG–84 file=yay0037
Positive Y-base error
80μ error
60μ error
Relative Intensity
1.05
1
0.95
0.9
0.85
0.8
0
100
200
300
400
500
Diode

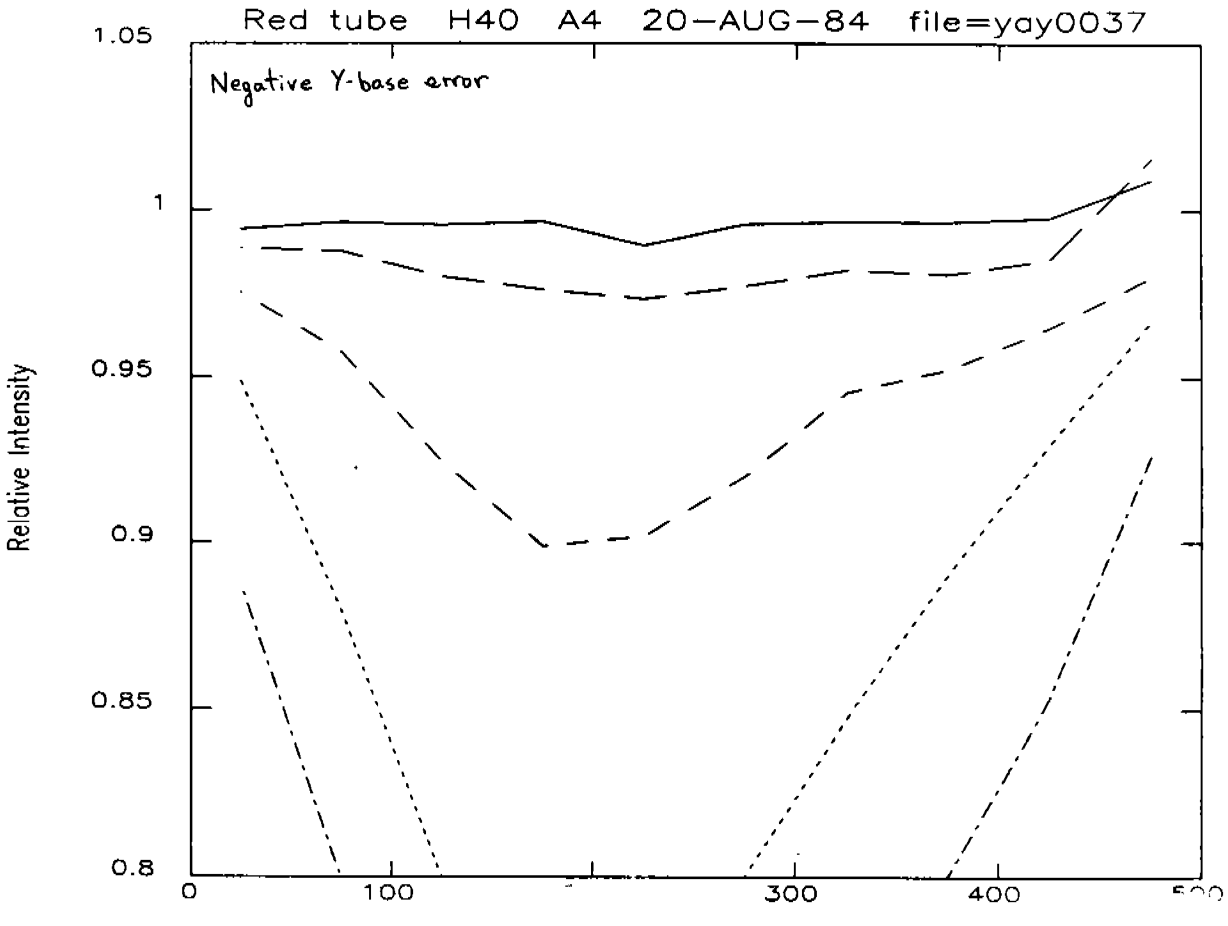
Red tube H40 A4 20–AUG–84 file=yay0037
Negative Y-base error
Relative Intensity
1.05
1
0.95
0.9
0.85
0.8
0
100
300
400

Figure 14.

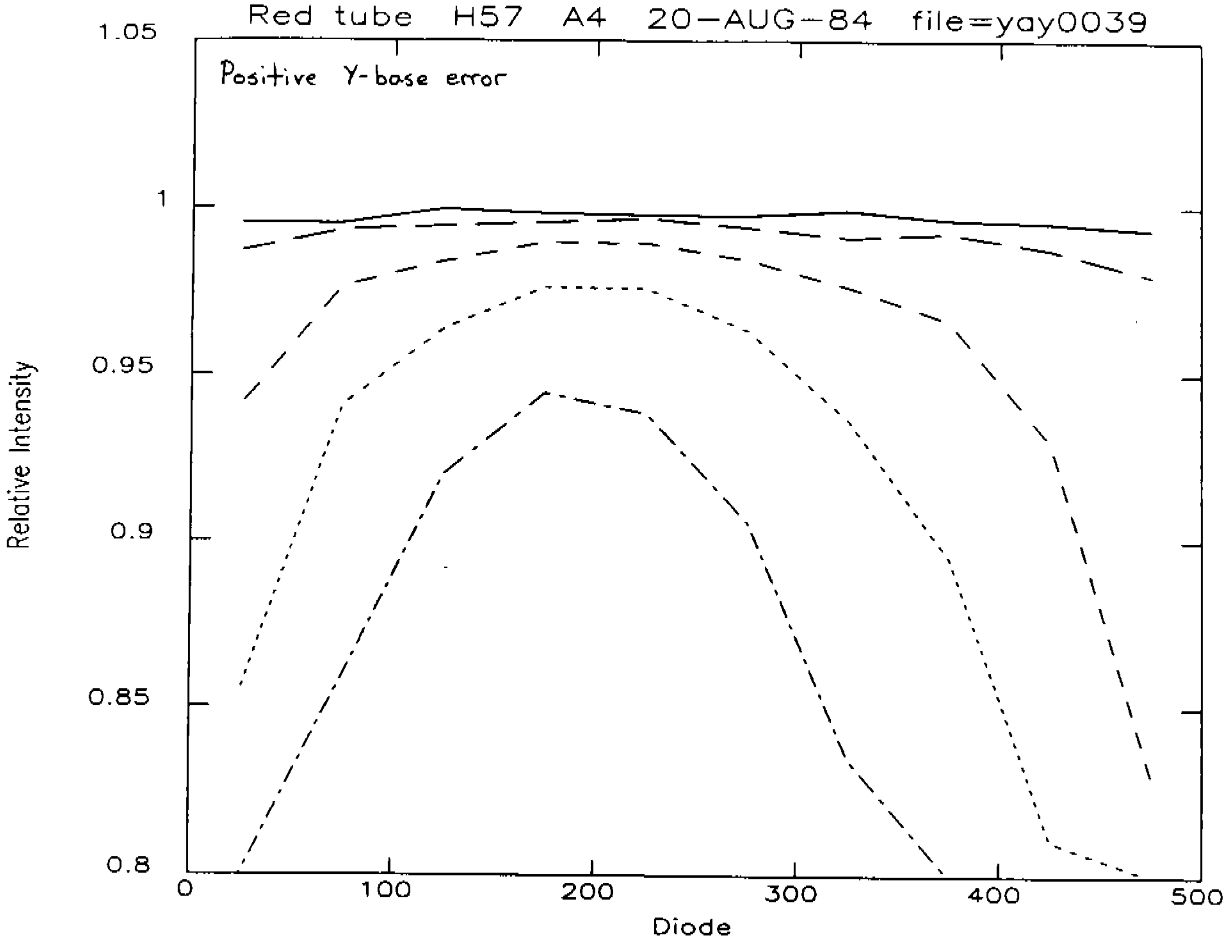

Red tube H57 A4 20-AUG-84 file=yay0039
Positive Y-base error
Relative Intensity
1.05
1
0.95
0.9
0.85
0.8
0
100
200
300
400
500
Diode

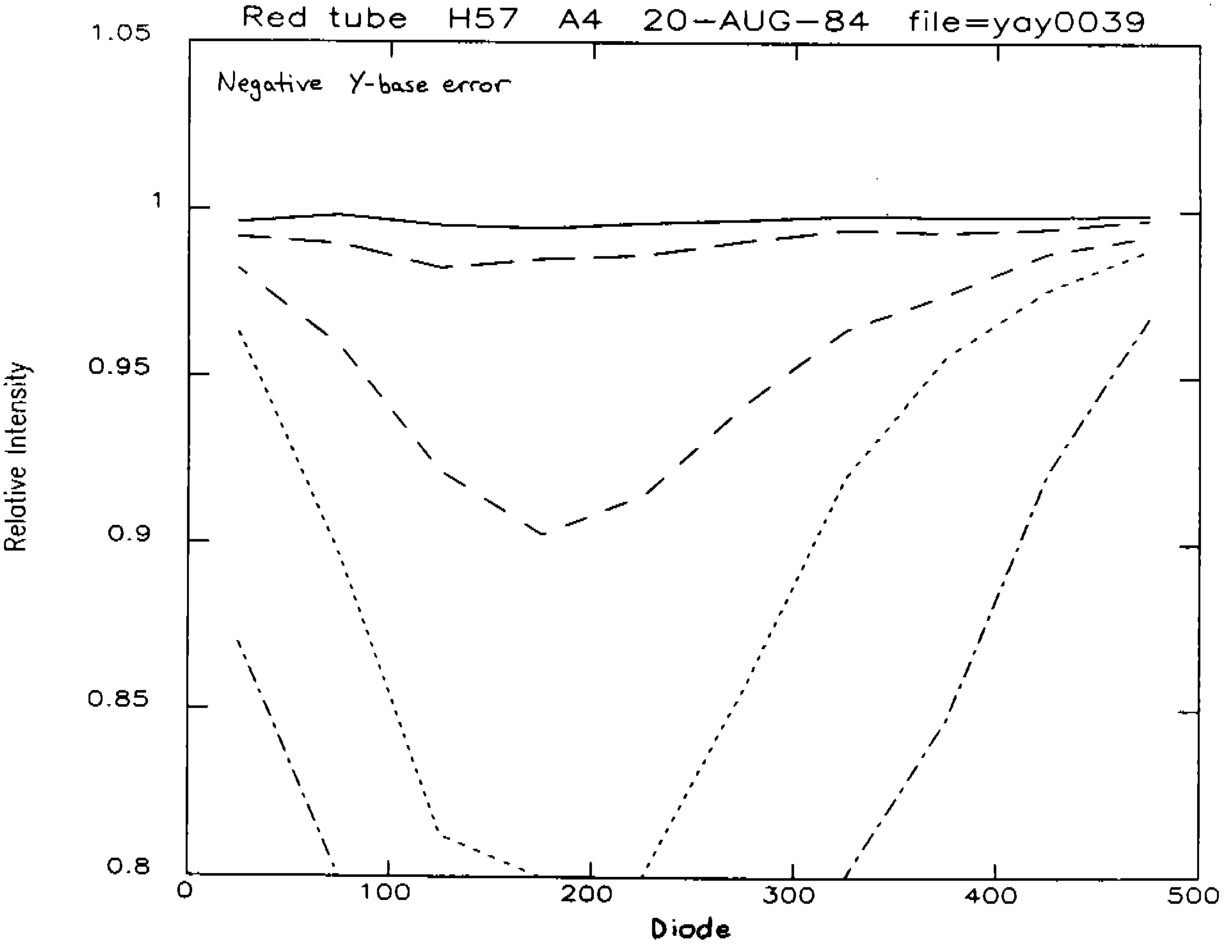

Red tube H57 A4 20-AUG-84 file=yay0039
Negative Y-base error
Relative Intensity
1.05
1
0.95
0.9
0.85
0.8
0
100
200
300
400
500
Diode

Figure 15.

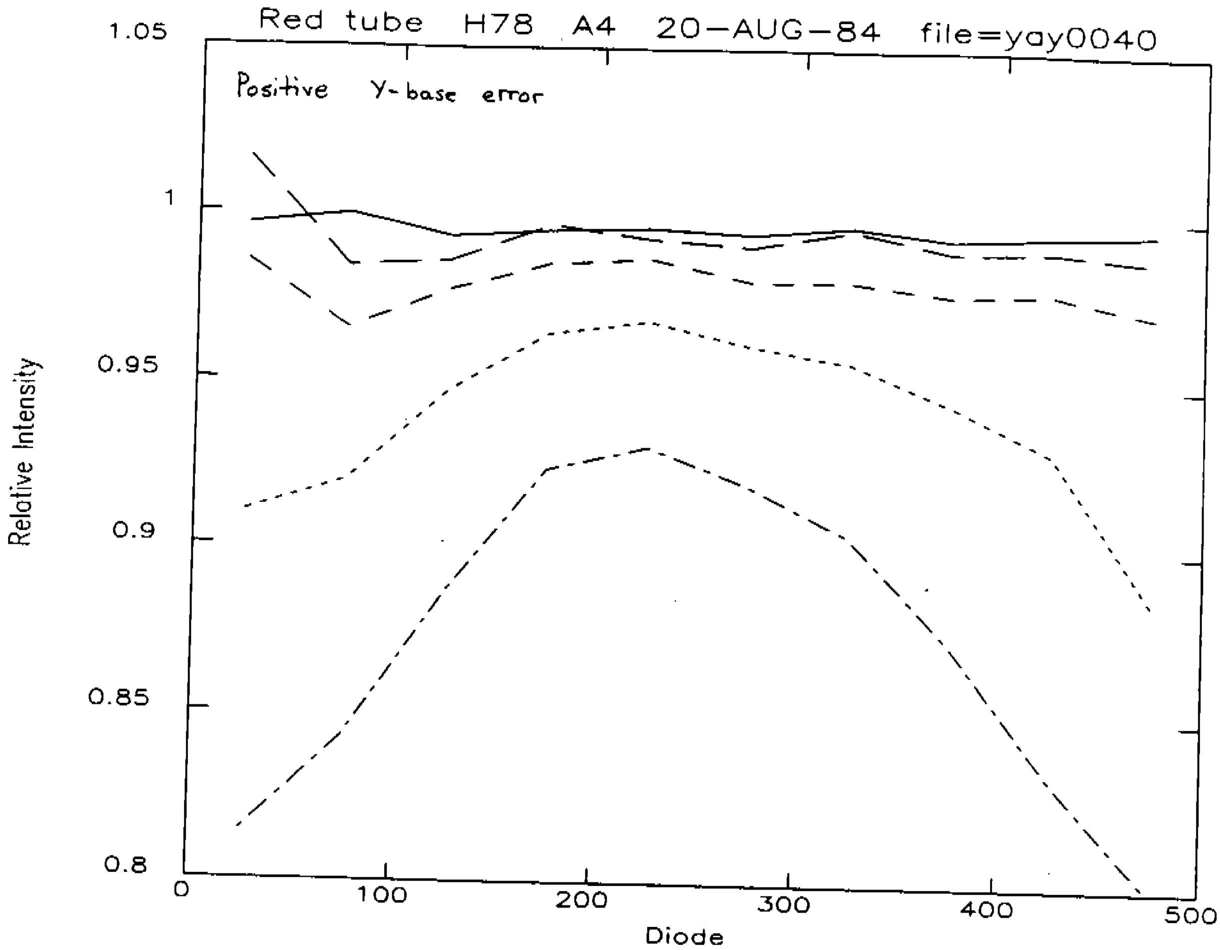
Red tube H78 A4 20-AUG-84 file=yay0040
Positive Y-base error
1.05
1
0.95
0.9
0.85
0.8
Relative Intensity
0
100
200
300
400
500
Diode

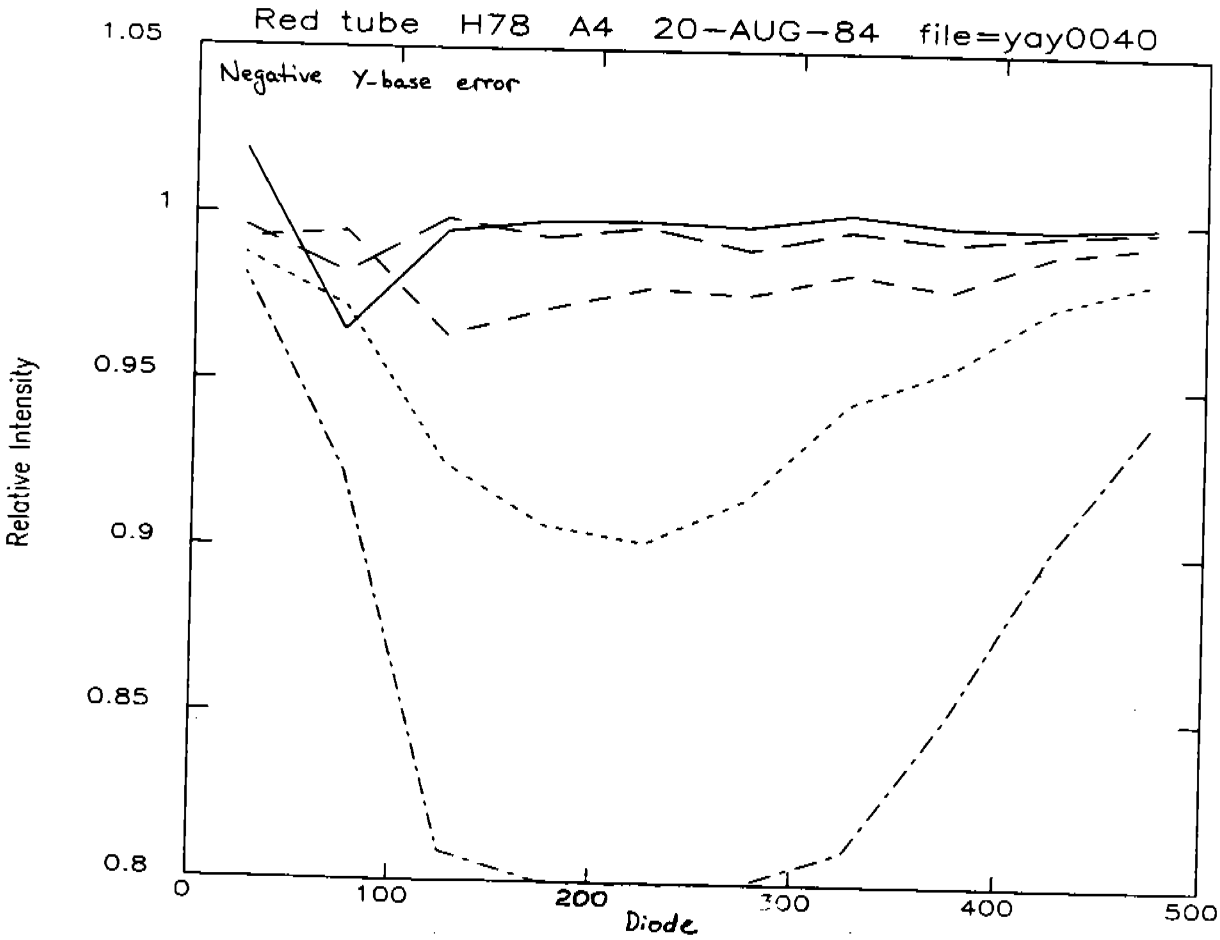
Red tube H78 A4 20-AUG-84 file=yay0040
Negative Y-base error
1.05
1
0.95
0.9
0.85
0.8
Relative Intensity
0
100
200
300
400
500
Diode